Structure-function relationships underpin disulfide loop cleavage-dependent activation of *Legionella pneumophila* lysophosholipase A PlaA

Miriam Hiller1#, Maurice Diwo2#, Sabrina Wamp1, Thomas Gutsmann3, Christina Lang1, Wulf Blankenfeldt2,4*, Antje Flieger1*

1 Division of Enteropathogenic Bacteria and Legionella (FG11), Robert Koch Institute, Burgstr. 37, 38855 Wernigerode, Germany.

2 Structure and Function of Proteins, Helmholtz Centre for Infection Research, Inhoffenstrasse 7, 38124 Braunschweig, Germany.

3 Research Center Borstel, Leibniz Lung Center, Division of Biophysics, Parkallee 10, 23845 Borstel, Germany; CSSB – Centre for Structural Systems Biology, Hamburg, Germany

4 Institute for Biochemistry, Biotechnology and Bioinformatics, Technische Universität Braunschweig, Braunschweig, Germany.

* corresponding authors: Antje Flieger and Wulf Blankenfeldt

Email: fliegera@rki.de and wulf.blankenfeldt@helmholtz-hzi.de;

# and * contributed equally

ORCID Antje Flieger 0000-0003-3819-2979, Sabrina Wamp 0000-0002-0387-4171,

Wulf Blankenfeldt: 0000-0001-9886-9668, Thomas Gutsmann: 0000-0001-5061-7891

Running title:

Activation of *Legionella pneumophila* lysophosholipase A PlaA

Keywords:

Legionella, phospholipase, GDSL enzyme, activation, 3D structure, disulphide loop, zinc metalloprotease

Abstract

Legionella pneumophila, the causative agent of a life-threatening pneumonia, intracellularly replicates in a specialized compartment in lung macrophages, the *Legionella*-containing vacuole (LCV). Secreted proteins of the pathogen govern important steps in the intracellular life cycle including bacterial egress. Among these is the type II secreted PlaA which, together with PlaC and PlaD, belongs to the GDSL phospholipase family found in *L. pneumophila*. PlaA shows lysophospholipase A (LPLA) activity which increases after secretion and subsequent processing by the zinc metalloproteinase ProA at residue E266/L267 located within a disulfide loop. Activity of PlaA contributes to the destabilization of the LCV in the absence of the type IVB-secreted effector SdhA. We here present the 3D structure of PlaA which shows a typical α/β hydrolase fold and reveals that the uncleaved disulfide loop forms a lid structure covering the catalytic triad S30/D278/H282. This leads to blockage of both substrate access and membrane interaction before activation; however, the catalytic and membrane interaction site gets accessible when the disulfide loop is processed. After structural modelling, a similar activation process is suggested for the GDSL hydrolase PlaC, but not for PlaD. Furthermore, the size of the PlaA substrate binding site indicated preference towards phospholipids comprising ~16 carbon fatty acid residues which was indeed verified by lipid hydrolysis, suggesting a molecular ruler mechanism. In conclusion, our analysis revealed the structural basis for the regulated activation and substrate preference of PlaA and suggests that protein activation of a potentially lytic enzyme may be important to maintain bacterial integrity.

63 **Introduction**

64

65 *Legionella pneumophila* is ubiquitously found in aqueous habitats, multiplies within environmental
66 amoebae, and is an important bacterial lung pathogen (1,2). From its natural habitat, *L. pneumophila* is
67 transmitted via aerosols into the human lung where lung macrophages serve as the primary replication
68 site. The infection process in mammalian cells and in amoeba shows many similarities. In both, the
69 bacteria apply means to withstand the multifaceted host defenses and subsequently replicate within a
70 specialized phagosome, termed the *Legionella*-containing vacuole (LCV) (3). Establishment of an intact
71 replication vacuole and its maintenance - for the time of bacterial replication - is essential for *Legionella*
72 propagation and requires a variety of bacterial and host factors (4,5). Several bacterial gene loci
73 contribute to intracellular establishment and replication of *L. pneumophila* and here secretion systems,
74 especially the type IVB (T4BSS) Dot/Icm and the type II (T2SS) Lsp systems, and their transported
75 effectors are major determinants (6-10). It has been shown that phospholipases are among the secreted
76 effectors and affect establishment and maintenance of the LCV. For example, patatin-like phospholipases
77 VipD and VpdC, both exported via the type IVB Dot/Icm machinery, influence lipid composition of
78 endosomes fusing to the LCV or vacuolar expansion by regulating lysophospholipid content, respectively
79 (11-14). Further, phospholipases are required to exit the LCV and the host after completed replication
80 and their involvement has been shown for a variety of pathogens including *L. pneumophila* (15-17).

81

82 Phospholipases are important virulence factors of pathogens (18) and classify into four major functional
83 groups based on the position at which they cleave within a phospholipid, specifically phospholipases A
84 (PLA), phospholipases B (PLB), phospholipases C (PLC), and phospholipases D (PLD). PLAs, like VipD or
85 VpdC, hydrolyze the carboxylester bonds at sn-1 or sn-2 position and thereby release fatty acids. If only
86 one fatty acid is targeted, a lysophospholipid is generated and may be further cleaved by a
87 lysophospholipase A (LPLA), liberating the remaining fatty acid. At least 19 phospholipases are found in
88 *L. pneumophila*, comprising 15 PLAs, three PLCs, and one PLD. The PLAs are divided into the patatin-like
89 phospholipases (incl. VipD), the PlaB-like, and the GDSL enzymes (19-21).

90

91 The *L. pneumophila* GDSL enzymes PlaA, PlaC, and PlaD, on which this study is focused, belong to the
92 family of GDSL hydrolases characterized by five conserved amino acid sequence blocks (19,22,23). The
93 first block is located near the N-terminus and contains the active site serine embedded in a Gly-Asp-Ser-
94 Leu (GDSL) motif as opposed to the Gly-X-Ser-X-Gly motif commonly found in other lipases. The catalytic
95 triad of GDSL hydrolases is completed by aspartate and histidine located in the fifth conserved block.

96 GDSL hydrolases have a flexible active site that allows for broad substrate specificity and enzyme
97 activities range from protease to arylesterase to PLA/LPLA and glycerophospholipid:cholesterol
98 acyltransferase (GCAT) activities. The latter transfers phospholipid-bound fatty acids to the acceptor
99 molecule cholesterol (22,23).
100
101 The three enzymes differ with regard to molecular weight, mode of secretion, and activity (Tab. 1). PlaA
102 and PlaC, which have molecular weights of 34.4 and 49.7 kDa, respectively, harbor a predicted sec SP
103 and are both secreted via the T2SS Lsp. PlaA mainly shows LPLA and GCAT activities while PlaC reveals
104 PLA and GCAT activities (24-26). PlaA LPLA but not GCAT activity and PlaC PLA and GCAT activities are
105 activated by zinc metalloproteinase ProA-dependent cleavage of a disulfide loop (26,27). However, the
106 mechanism is not understood from a structure-centered view. The 59.6 kDa protein PlaD has not been
107 characterized extensively, lacks a predicted sec secretion signal, and it is not secreted into the culture
108 supernatant upon growth in broth medium (27).
109
110 Relevance of PlaA and PlaC during host cell infection was shown for both enzymes. Specifically, in the
111 absence of the T4BSS effector SdhA, which is important for LCV stabilization, PlaA can disrupt the
112 vacuole membrane such that the bacteria get access to the cytosol, i.e. prematurely egress from the LCV
113 and, as a consequence, host cell death pathways are triggered (15,28). Further, a *L. pneumophila* GDSL
114 triple mutant showed reduced cell exit (17). Therefore, PlaA may be an important factor supporting
115 bacterial LCV and host egress after intracellular replication. In line with these functions, PlaA and its
116 activity is detected from mid-exponential growth phase on and is most prominent in late-logarithmic
117 growth phase (29,30). Also, PlaC is more abundant during stationary phase than during logarithmic
118 growth phase and shows a functional overlap with the aminopeptidase LapA (30,31). Although *plaC* and
119 *lapA* individually seemed dispensable for host infections, *L. pneumophila plaC/lapA* double mutants
120 show a severe replication defect in *Acanthamoeba castellanii* (31).
121
122 Since many of the pathogen phospholipases are capable to attack cellular membranes, such enzymes
123 may also damage the pathogen itself before export from the pathogen. Therefore, sophisticated
124 activation mechanisms might be required for example to prevent self-inflicted damage to the producer
125 or to spacially regulate activity. Such mechanisms are multifaceted and include the following: 1)
126 oligomerization as found in *E. coli* PldA (32), 2) deoligomerization as described for *L. pneumophila* PlaB or
127 *P. aeruginosa* PlaF (21,33,34), interaction with accessory factors, such as 3) metal ions described for *L.*
128 *pneumophila* PLCs (35), 4) chemical modification, such as ubiquitination of VpdC (14), or 5) host or

129 bacterial protein cofactors, as Rab5/Rab22 found for *L. pneumophila* VipD (11-13), and 6) proteolytic
130 processing of proenzymes. The latter proteolysis-based activation is described for *L. pneumophila* PlaA
131 and PlaC (26,27,36). Both enzymes contain a disulfide loop within the C-terminal half which is
132 proteolytically processed by the type II-secreted zinc metalloproteinase ProA. ProA processing
133 substantially increases the activities of PlaA and PlaC and truncation of the disulfide loop generates
134 enzymes that are highly active independent of ProA (26,27). These data highlight proteolytic activation
135 of these enzymes by elimination of a disulfide loop which in the uncleaved form may hinder substrate
136 access to the catalytic triad.
137
138 We present here the crystal structure of PlaA as basis for the clarification of structure-function
139 relationships in disulfide loop cleavage-dependent enzyme activation. The PlaA structure is moreover
140 compared to computational models of PlaC and PlaD to highlight similarities and differences between
141 these enzymes. Thus, we establish a link between structure and enzymatic function of PlaA.

142 **Results**

143 **PlaA displays a classical α/β-hydrolase fold containing the catalytic triad S30/D278/H282**

144 The gene for PlaA without the respective predicted N-terminal SP (amino acids 1-18) was expressed in
145 *E. coli* and purified via an N-terminal Strep-tag. After size exclusion chromatography (SEC), the protein
146 was subjected to crystallization. PlaA crystallized in spacegroup $P3_121$ with one chain of the monomeric
147 protein in the asymmetric unit. This crystal form differs from a previous report where PlaA has been
148 crystalized in space groups $P2_1$ and $P2_12_12_1$ but where structure determination has remained pending
149 (37). Initial phases were obtained from single-wavelength anomalous diffraction data collected at an X-
150 ray energy of 7 keV (wavelength = 1.7712 Å) of a crystal obtained in the presence of ammonium iodide
151 (Fig. S1A and B). Crystallization in the presence of 1-monopalmitoyllysophosphatidylcholine (16:0 LPC)
152 and avoiding polyethylenglycol (PEG) in the precipitant led to crystals of the same spacegroup (Fig. S1A)
153 and no significant structural differences were observed between the crystal structures determined in this
154 study. With the exception of a few residues at the N- and C-termini as well as parts of a highly flexible
155 surface loop (residues V91 – E92), the final structures show all of the PlaA protein (Fig. 1A). The N-
156 terminal Strep-tag was too flexible to produce traceable electron density. The highest resolution
157 obtained here is 1.45 Å for PlaA complexed with the 16:0 LPC hydrolysis product palmitate (Fig. S1B). The
158 structures substantiate that PlaA is a canonical GDSL hydrolase with a typical α/β-hydrolase fold (Fig. 1A).
159 The catalytic triad was previously determined as S30, D278, H282 by means of mutational analysis (27)
160 and is confirmed in the 3D structure. The central β-sheet consists of five parallel β-strands and is
161 surrounded by a set of α-helices on both of its sides (Fig. 1A, Fig. S1C). The N-terminus and the C-
162 terminus of PlaA (shown in blue and red in Fig. 1A) are located in close proximity to each other.

163

164 **Detection of a hydrophobic channel that matches with linear fatty acids of 16 carbon atoms in close**
165 **proximity to the catalytic triad and importance of substrate and product analogues for crystallization**

166 Interestingly, crystallization was initially only possible in the presence of PEG. Here, we observed
167 additional electron density in a hydrophobic channel in close proximity to the catalytic triad (Fig. S1D),
168 despite the fact that this channel is not accessible from the solvent. The channel has a length of approx.
169 20 Å, suggesting that the unexplained electron density derives from a molecule that mimics the fatty acid
170 moiety of the substrate such as short unbranched PEG components of the precipitant used to crystallize
171 the protein. We hence interpreted the additional electron density as a fragment of PEG. Subsequently,
172 we aimed for the structure of a complex of PlaA with its substrate 16:0 LPC by co-crystallization in a PEG-
173 free precipitant. This yielded crystals of the same space group (Fig. S1A) that diffracted to 1.45 Å

174 resolution. Here, we observed additional electron density that occupies the entire hydrophobic channel
175 (Fig. S1E). This density was interpreted as the product of PlaA-dependent hydrolysis of 16:0 LPC, palmitic
176 acid (Fig. 1B). Interestingly, no crystals were obtained in the absence of substrate (16:0 LPC) or product
177 analogues (palmitate, PEG), which may point towards higher flexibility of apo-PlaA. This flexibility may
178 include partial unfolding for hydrophobic substrate binding.
179
180 **A disulfide loop functions as a lid that covers the catalytic triad and reduces membrane interaction**
181 **before enzyme activation**
182 Regarding potential structural elements hindering substrate binding in the non-activated state of PlaA, a
183 disulfide loop (from C243 to C272; shown in orange in Fig. 1A and in yellow in Fig. 1C, respectively)
184 covers the entrance to the substrate binding pocket and the catalytic triad of PlaA. It is therefore
185 conceivable that ProA-mediated hydrolytic processing of the disulfide loop facilitates access of
186 substrates to the binding pocket and to the active site, explaining the increased LPLA activity upon
187 exposure to ProA. The previously determined proteolytic maturation site E266/L267 at the C-terminal
188 end of the lid (27) is solvent accessible in the crystal structure (Fig. 1A). Parts of the lid display high B-
189 factors, indicating that they are relatively mobile. We therefore propose that proteolytic maturation by
190 ProA increases flexibility further and enables parts of the lid to leave the position as observed in the
191 crystal structure. This would open up the entry to the active site and is in line with proteolytic activation
192 mechanism of other lipases (38).
193
194 Among others, DALI (39) searches identify the cholin esterase ChoE from *P. aeruginosa* (PDB code 6uqv)
195 (40), the phospholipase PlpA from *Vibrio vulnificus* (PDB code 6jl2) (41), or the esterase domain of
196 autotransporter EstA from *P. aeruginosa* (PDB code 3kvn) (42) as highly structurally similar to PlaA (Fig.
197 2A-D). Interestingly, while these proteins also possess disulfide loops in similar positions, these disulfide
198 loops are shorter in sequence and they do not shield the active center as much as the disulfide loop of
199 PlaA in the unprocessed state observed here (Fig. 2). As a consequence, the ligand binding sites of these
200 enzymes are solvent accessible, suggesting that they do not require proteolytic activation.
201
202 We further analyzed whether membrane interaction of PlaA is influenced by disulfide loop processing
203 and tested the catalytic inactive variant (PlaA S30N) versus the respective disulfide loop mutant (PlaA
204 S30N Δaa247-268), which possesses increased enzyme activity similar to the ProA-processed protein
205 (27), in a Förster-Resonance Energy Transfer (FRET) liposome-insertion assay. When protein-lipid
206 interaction exceeds peripheral binding and proteins at least insert into the lipid headgroup region, this

207 leads to an increase in the distance between the fluorophores and thus to reduced energy transfer.
208 Consequently, the ratio of donor and acceptor fluorescence intensities is a measure of protein insertion
209 into membranes. Indeed, a higher ratio and therefore substantial membrane insertion was observed for
210 the disulfide loop deficient mutant PlaA S30N Δaa247-268 compared to PlaA S30N (Fig. 3). This indicates
211 that the disulfide lid reduces lipid interaction; or in other words, lipid interaction is facilitated by disulfide
212 loop cleavage which might also impact enzyme activity.
213
214 **Substrate selectivity of PlaA concerning fatty acid chain length is governed by a molecular ruler**
215 **mechanism**
216 As mentioned above, we observed unexplained elongated electron density in the ligand binding site of
217 the first high-resolution structure of PlaA and attributed this to a PEG fragment deriving from the
218 precipitant solution (Fig. S1D). However, this molecule did not fill the binding site completely, and
219 further structural analysis suggested that PlaA can accommodate phospholipid substrates with linear
220 fatty acid chains of at least 16 carbon atoms length, which was then confirmed with the crystal structure
221 of PlaA in complex with palmitate (Fig. 1B, Fig. S1E). To further investigate the substrate spectrum of
222 PlaA, we tested whether LPLA activity of PlaA correlated with the length of the fatty acid chains. To this
223 end, PlaA was incubated with lysophosphatidylcholine (LPC) with diverse fatty acid residues. These
224 varied in length from eight to 22 carbon atoms. PlaA in its unprocessed form only exhibited some
225 detectable activity towards 16:0 LPC (Fig. 4A). Additionally, activity was compared to the disulfide loop-
226 deleted PlaA ΔAA247-68, which corresponds to ProA-processed PlaA (27). The LPLA activity of PlaA
227 ΔAA247-68 was distinctly higher than that of uncleaved PlaA and was mainly directed towards 16:0 LPC,
228 but 8:0 LPC, 12:0 LPC, and 18:0 LPC were also hydrolyzed to a lower extent. As hypothesized, no activity
229 towards 20:0 LPC and 22:0 LPC was observed for both PlaA proteins. PlaA variants with mutation of the
230 catalytic serine Ser30 (rPlaA S30N and rPlaA S30N ΔAA247-68) were used as controls and did not exhibit
231 activity towards any of the tested lipid substrates (Fig. 4A). These findings suggest that the substrate
232 selectivity of PlaA is governed by a molecular ruler mechanism (43).
233
234 **During growth of *L. pneumophila* in liquid culture, PlaA is first present in its unprocessed form until**
235 **ProA is secreted in sufficient amounts for PlaA processing**
236 PlaA is a type II-secreted protein found in culture supernatants of *L. pneumophila* (24,25,27). We were
237 interested if and when ProA-processing of PlaA occurs in *L. pneumophila* grown in liquid cultures (Fig. 4B-
238 D). PlaA was detected as 35 kDa full-length protein during lag and logarithmic growth phases with a
239 maximum quantity at 2 to 3 h of growth. During mid-exponential growth, from ~4 h of incubation,

240 processed PlaA with a molecular weight of ~25 kDa (Tab. 1) was detected for the first time and from 5h
241 remained the only PlaA version until late logarithmic / stationary phase (Fig. 4B and C). These
242 observations correlated with an accumulation of ProA in the culture supernatants over time (Fig. 4D). In
243 conclusion, our experiments indicate that after secretion of sufficient amounts of ProA, PlaA is processed
244 into its activated form.
245
246 **PlaA activation by ProA-dependent cleavage is not inhibited by mutation of the preferred cleavage site**
247 **E266/L267 highlighting broader cleavage site acceptance by ProA**
248 As outlined above, an important feature of PlaA is a disulfide loop lid structure and after its processing
249 access of lipid substrates to the catalytic active site and protein-lipid interaction is facilitated and thus
250 leads to an increase of the LPLA activity. We previously reported that this disulfide loop is cleaved by the
251 *L. pneumophila* zinc metalloproteinase ProA at the preferred cleavage site E266/L267, resulting in an
252 increase of the LPLA activity. Also, complete removal of the disulfide loop in PlaA ΔAA247-68 yields fully
253 active PlaA and similar activity characteristics as ProA-processed PlaA (27). Subsequently, we analyzed
254 whether mutation of the main cleavage site E266/L267 may hinder PlaA activation. We found that the
255 mutation of E266/L267 into N266/N267 is not sufficient to prevent ProA-dependent increase in LPLA
256 activity of PlaA by proteolytic processing indicating that ProA may attack other exposed residues
257 surrounding the major cleavage site in the disulfide loop (Fig. 4E). This was indeed implied by peptide
258 mapping of PlaA digested by ProA which identified additional but less preferred cleavage sites, such as
259 K264/P265, P265/E266, and L267/T268, directly upstream and downstream of the preferred cleavage
260 site (27). This further highlights the broad cleavage site acceptance by ProA (44).
261
262 **Comparison of PlaA to structural models of PlaC and PlaD highlights the presence of catalytic site**
263 **covering disulfide loops shielding the catalytic side in PlaC but not PlaD. Similar hydrophobic channel**
264 **lengths are found in PlaA, PlaC, and PlaD.**
265 To obtain additional insight into the structure of the three *L. pneumophila* GSDL phospholipases, we
266 generated structural models of PlaC and PlaD using the template-free routine of AlphaFold (45). The
267 structure of PlaA was predicted as well to evaluate the method, and no significant differences were
268 found with respect to the X-ray structures described above (Fig. 5A, Fig. S2A-C). Notably, this also
269 includes the more flexible parts of PlaA (residues V91 – E97 and the disulfide loop), whose flexibility is
270 correctly indicated by a lower confidence score. Importantly, the predicted conformation of the disulfide
271 loop matches the crystal structure very well (Fig. S2A-C).

272

273 Compared to PlaA, PlaC although similar in structure is predicted to contain additional helical elements
274 in P57 – G120 and D166 – P193 which correspond to its larger size (Fig. 5B). Of these, the second region
275 replaces the flexible region V91 – D95 of PlaA. Similar to PlaA, PlaC has a lid domain that is delimited by a
276 disulfide bridge (C343-C388) which accommodates the proteolytic maturation site (27). In PlaC, this lid
277 includes an α-helix (362-370) that shields the active site from the solvent. However, this α-helix is slightly
278 shifted away from the active site, resulting in a larger entrance funnel for PlaC possibly explaining
279 differences in the substrate specificity of both enzymes. While PlaA preferentially hydrolyzes
280 lysophospholipids, PlaC also accepts larger substrates such as diacyl phospholipids (26). The length of
281 PlaC's hydrophobic substrate channel is identical to PlaA's, indicating that in both cases linear fatty acids
282 with 16 carbon atoms are the preferred substrates.

283

284 The structure of PlaD includes the α/β hydrolase domain (N-terminal domain) and is predicted to have an
285 additional α-helical domain of unknown function at its C-terminus (P403 – T516) (Fig. 5C). The relative
286 orientation towards the α/β-hydrolase domain is unclear at present since both domains are connected
287 by a long flexible linker (P371 - L402). Comparison with PlaA reveals additional helical elements (e.g. P60
288 – P72). Importantly, PlaD does not contain a disulfide loop, and the respective region of the protein
289 (Y311 – A334, shown in light blue in Fig. 5C) is predicted to adopt an open conformation that leads to an
290 unshielded substrate binding site. In addition to differences in protein secretion, these features may
291 explain further possible differences in the activation mechanism of this protein compared to PlaA and
292 PlaC. The length of the hydrophobic substrate channel of PlaD, on the other hand, is identical to that of
293 PlaA, again suggesting preference for linear fatty acids with 16 carbon atoms.

294

295

296 **Discussion**

297

298 Here we show that PlaA, which is one of three proteins of the GDSL phospholipase family found in *L.*
299 *pneumophila* (19), adopts an α/β hydrolase fold typically found in similar enzymes of other bacteria, such
300 as the cholin esterase ChoE from *Pseudomonas aeruginosa* (PDB code 6uqv), the phospholipase PlpA
301 from *Vibrio vulnificus* (PDB code 6jl2), or the esterase domain of autotransporter EstA from *P. aeruginosa*
302 (PDB code 3kvn) to name just a few examples (Fig. 2) However, PlaA also shows specific features which
303 relate to its activation mechanism and substrate specificity. Structural analysis reveals that a disulfide
304 loop lid structure blocks substrate access to the catalytic site in ProA-unprocessed PlaA. The active site
305 gets accessible when the disulfide loop is opened up by proteolysis. After structural modelling using
306 AlphaFold, a similar activation mechanism is suggested for PlaC but not for PlaD, where the catalytic site
307 seemed freely accessible as further observed in ChoE, PlpA, and EstA (Fig. 2).

308

309 Lid structures are very common in lipases and are important for substrate specificity and control of
310 enzymatic activity (46). It can be assumed that processing of the PlaA disulfide loop by ProA might
311 completely remove the lid or at least increase its flexibility. This might affect the conformation of the
312 active site or the potential substrate-binding domain or both. It is conceivable that the access of lipid
313 substrates to the active site channel of PlaA is facilitated by the structural alterations induced by ProA-
314 dependent processing, which might explain the increased LPLA activity of processed PlaA. Proteolytic
315 processing is a common mechanism for activation of enzymes that have been produced as inactive
316 zymogens (38). Among others, the induction of enzymatic activity after processing within a disulfide loop
317 has been shown for some, such as *Pseudomonas* exotoxin A and Shiga toxin from enterohemorrhagic
318 *Escherichia coli* (47-50). Although unprocessed PlaA is not completely inactive, it can be assumed that
319 the rationale of ProA-dependent regulation of PlaA is to increase the enzymatic activity only after PlaA is
320 secreted to the exterior and at the required time point. Since phospholipase activities are potentially
321 harmful to the bacterium itself, we propose that the here presented activation mechanism is used to
322 avoid self-inflicted lysis from a lytic enzyme before secretion to the exterior.

323

324 *L. pneumophila* is an intracellularly replicating lung pathogen which induces major lung damage leading
325 to a severe pneumonia and the secreted bacterial phospholipases may contribute to the clinical picture
326 (2,19). Eukaryotic membranes and the surfactant phospholipid monolayer in the lung contain major
327 amounts of phospholipids with esterified fatty acids of a length of ~16 carbon atoms (51). We showed
328 that the size of an intramolecular channel in PlaA, PlaC, and PlaD nicely fits to harbor such lipids and also

329 the reaction product palmitic acid (Fig. 1B) which mechanistically underlines host-adapted substrate
330 specificity of these enzymes.
331
332 Interestingly, it was shown that PlaA is responsible for the destabilization of the LCV in the absence of
333 the T4BSS secreted effector SdhA, which localizes to the LCV (15). SdhA-deficient *L. pneumophila* is
334 unable to replicate in murine bone-marrow derived macrophages due to impairment of LCV stability with
335 subsequent induction of host cell death pathways (15,52). This phenotype was rescued by the additional
336 deletion of PlaA (15). The mechanism of SdhA action has recently been shown as binding and blocking
337 the function of OCRL (OculoCerebroRenal syndrome of Lowe), an inositol 5-phosphatase pivotal for
338 controlling endosomal dynamics and participating in vacuole disruption. Accordingly, OCRL depletion
339 results in enhanced vacuole integrity and intracellular growth of a *L. pneumophila sdhA* mutant (28). A
340 similar interplay occurs in *Salmonella enterica* spp. *enterica* serovar Typhimurium where the SPI2 type III-
341 secreted effector SseJ, which shows homology to PlaA, destabilizes the vacuolar membrane in the
342 absence of SifA, another SPI2 effector (53). In general, it is important for intracellular pathogens to
343 maintain the integrity of the replication vacuole to avoid detection by the immune system of the host
344 (54). However, for the exit of the pathogen and the initiation of a new infection cycle, the vacuole needs
345 to be disrupted (16). Assuming that the functions of SdhA and PlaA are opposed and must be balanced
346 for maintenance of the LCV integrity for the period of bacterial replication (54), it may be that a change
347 of abundance or activity of either factor could result in exit of *L. pneumophila* from the LCV and
348 subsequently the host cell. The here addressed increase of PlaA activity and membrane interaction by
349 proteolytic activation could disturb the balance between SdhA and PlaA in an infection and might thus
350 lead to destabilization of the LCV triggering the exit process.
351
352 The kinetics of PlaA processing and activity *in vivo* have not been described previously. Our analyses of
353 culture supernatants at multiple time points during *L. pneumophila* growth in liquid medium revealed
354 that PlaA is initially secreted as full-length protein. Processing was first detected during mid-exponential
355 growth. We speculate that ProA-processing of PlaA does not occur before a critical density of
356 intravacuolar bacteria is reached which produces sufficient ProA quantities. In parallel, a similar process
357 is plausible for proteolytic activation of PlaC which might allow cooperation of PlaC, majorly revealing
358 PLA, and PlaA, majorly possessing LPLA activity. Thus, this mechanism might lead to the activation of
359 enzyme activities as a function of cell density in similarity to the regulatory process of quorum sensing
360 (55). In this manner destabilization of the LCV for host exit can be linked to a high cell density and
361 completed bacterial replication.

362

363 Together, these findings provide insight into the relationship between structure and activity of PlaA and
364 for the other GSDL hydrolases in *L. pneumophila*. We found that these enzymes possess structural
365 features that may lead to a specific activity and activation profile tailored to the needs of the bacterium.

366

367

368

369

370

371

372 **Experimental procedures**

373

374 **Bacterial strains and growth conditions**

375 All experiments and sequence or structure predictions were performed with *L. pneumophila* sg1 strain
376 Corby including recombinant gene expression in *E. coli* BL21. The strains used and generated in the study
377 are listed in Tab. 2. *L. pneumophila* strains were grown on buffered charcoal yeast extract (BCYE) agar
378 and in buffered yeast extract (BYE) broth and *E. coli* strains were grown on Luria Bertani (LB) agar and in
379 LB broth as described previously (36,56,57). If appropriate, 100 µg/ml ampicillin or 50 µg/ml kanamycin
380 were added to *E. coli* cultures.

381

382 **Construction of plasmids**

383 The vector pMH42 was generated from pMH41 by means of the QuikChange Site-Directed Mutagenesis
384 Kit (Stratagene) using the primers PlaA_S30N_fw (5'-GTATTTGGTGATAATTTGTCGGATAACGG-3') and PlaA
385 S30N_rv (5'-CCGTTATCCGACAAATTATCACCAAATAC-3') for introduction of the S30N point mutation in
386 *plaA* (Tab. 2). Primers were obtained from Eurofins MWG Operon and Integrated DNA Technologies. All
387 restriction enzymes were obtained from New England Biolabs. Plasmid DNA was introduced into *E. coli*
388 by heat shock transformation.

389

390 **Expression and purification of recombinant PlaA for enzyme activity tests and analysis of crystal**
391 **structure. Expression and purification of recombinant ProA.**

392 *E. coli* BL21 strains harboring plasmids for recombinant expression of *plaA* variants without SP and N-
393 terminally fused Strep-tag (Tab. 2) were grown in LB broth supplemented with ampicillin at 37 °C and
394 250 rpm to an OD_{600} = 0.8, induced with 0.1 mM IPTG, and transferred to 18 °C and 250 rpm for 16 – 17
395 h. The bacterial pellet was collected and resuspended in 100 mM Tris-HCl, pH 8.0, containing 100 mM
396 NaCl. Homogenization was performed with Emulsi Flex C3 (Avestin) applying 25,000 to 30,000 psi. The
397 soluble fraction was collected by centrifugation at 13,000 g and 4 °C for 60 min. Strep-PlaA and variants
398 were purified using Strep-Tactin Superflow high capacity resin (IBA) and further purified by SEC
399 (Superdex S200 10/30 Increase) performed with SEC buffer (20 mM Tris pH 8, 150 mM NaCl, 1 mM DTT)
400 according to the manufacturer's instructions. Recombinant periplasmic ProA was isolated by osmotic
401 shock from *E. coli* BL21 (pCL15) and subsequent anion exchange chromatography (26).

402

403 **Crystallization, X-ray diffraction, and structure determination**

404 Crystals were obtained by sitting drop vapor diffusion at 20 °C. Initially, 200 nl PlaA solution at 8 mg/mL
405 in SEC buffer were mixed with 200 nl of 14.7% (w/v) PEG3350, 1% (w/v) PEG 1K, 0.5% (w/v) PEG200,
406 8.9% (v/v) tacsimate pH 5, 200 mM NH_4I, 1 mM $CaCl_2$, and 1 mM $MgCl_2$. For cryoprotection, crystals were
407 briefly washed in a solution of 10% (v/v) (2R,3R)-(−)-2,3-butandiole, 16% (w/v) PEG3350, 6% (v/v)
408 Tacsimate pH 5, and 920 mM NH_4I. To exploit the f'/f'' difference arising from the L I absorption edge of
409 iodine (5.1881 keV, 2.3898 Å), two datasets at an X-ray energy of 7.000 keV (λ = 1.771196 Å) and with
410 detector distances of 140 mm and 135 mm were collected at beamline X06DA (PXIII) of the Swiss Light
411 Source (SLS; Villigen, Switzerland) (58). These data were indexed, scaled and merged with autoproc (59)
412 and then used for initial phasing by single anomalous dispersion (SAD) analysis through hkl2map and the
413 SHELX-package (60) The resulting poly-alanine model served as a template for phenix.autobuild (61).
414 Manual editing was done in Coot (62) from the CCP4 software suite (63). Structure refinement was done
415 with phenix.refine and pdb-redo (64,65). 13 iodide anions were placed in the final model (Fig. S1B).
416 High resolution data of a crystal obtained under similar conditions were collected at the same beamline,
417 using an X-ray wavelength of 1.3778 Å. Diffraction data of a crystal grown from 7 mg/mL PlaA solution in
418 SEC buffer supplemented with 500 µM 1-monopalmitoyllysophosphatidylcholine (16:0 LPC) with a
419 precipitant consisting of 2.2 M $(NH_4)_2SO_4$ and 0.2 M NH_4-acetate were collected on beamline P11 of the
420 PETRAIII synchrotron (DESY Hamburg, Germany) (66). The cryoprotectant consisted of precipitant
421 solution supplemented with 10% (v/v) (2R,3R)-(−)-2,3-butandiole in this case. Refinement proceeded via
422 Fourier synthesis followed by employing the same methods as in the case for the SAD structure (specific
423 data see Tab. 3).
424
425 **Prediction of 3D structures of PlaA, PlaC and PlaD**
426 The 3D structures of PlaA (gene lpc1811), PlaC (gene lpc3121) und PlaD (gene lpc0558) were predicted
427 using the template-less routine of AlphaFold (45) through a local installation of ColabFold (67). The
428 required protein sequences were obtained from NCBI.
429
430 ***In vitro* analysis of lipolytic activity and proteolytic processing of recombinant PlaA**
431 Lipolytic activities of recombinant PlaA variants were investigated as described previously (25,36,68). The
432 lipid substrates 1,2-dipalmitoylphosphatidyl-glycerol (PG), 1,2-dipalmitoylphosphatidylcholine (PC), 1-
433 mono-palmitoyllysophosphatidylglycerol (LPG), 1-monooctanoyllysophosphatidylcholine (8:0 LPC), 1-
434 monolauroyllysophosphatidylcholine (12:0 LPC), 1-monopalmitoyllysophosphatidylcholine (LPC or
435 16:0 LPC), 1-monostearoyllysophosphatidylcholine (18:0 LPC), 1-monoarachidoyllysophosphatidylcholine
436 (20:0 LPC), and 1-monobehenoyllysophosphatidylcholine (22:0 LPC) were applied for the assays. Briefly,

437 25 ng of recombinant protein were incubated with 6.7 mM lipid suspensions with or without addition of
438 3.5 mU ProA at 37 °C for the indicated time followed by quantitative detection of free fatty acids (FFA).
439

440 **FRET liposome-interaction assay**

441 Förster Resonance Energy Transfer Spectroscopy—insertion of PlaA proteins into liposome membranes
442 was determined in 40 mM Tris, 150 mM NaCl, pH 7.5, at 37 °C by FRET spectroscopy applied as a probe
443 dilution assay (69). L-α-phosphatidylcholine (ePC, 95%, chicken egg) and L-α-phosphatidylethanolamine
444 (ecPE, *E. coli*) were purchased from Avanti (Avanti Polar Lipids Inc., Alabaster, AL, USA) and prepared at
445 stock concentrations of 10 mg/mL in $CHCl_3$. Fluorescence conjugated lipids
446 *N*-(7-nitrobenz-2-oxa-1,3-diazol-4-yl)-1,2-dihexadecanoyl-*sn*-glycero-3-phosphoethanolamine (NBD-PE)
447 and Lissamine™ Rhodamine B 1,2-dihexadecanoyl-*sn*-glycero-3-phosphoethanolamine (Rho-DHPE), were
448 purchased from Life Technologies (Carlsbad, CA, USA). Proteins were added to PC:PE (1:1) liposomes,
449 which were labelled with 1% of the donor NBD-PE and 1% of the acceptor rhodamine-PE. The
450 fluorescence was measured by means of a spectrometer (Fluorolog 3, Horiba Jobin Yvon GmbH,
451 Bensheim, Germany). NBD excitation wavelength was 470 nm. Protein insertion was monitored as the
452 increase of the ratio of the donor fluorescence intensity I_{donor} at 531 nm to that of the acceptor intensity
453 $I_{acceptor}$ at 593 nm. This ratio depends on the Förster efficiency; therefore, a ratio > 1 highlights that the
454 mean distance of donor and acceptor dyes increased. Values were determined 60 min after addition of
455 100 µg/ml protein. Buffer (see above) was used to dilute the proteins and control.
456

457 **Analysis of processing status of PlaA from *L. pneumophila***

458 Overnight cultures of *L. pneumophila* sg1 strain Corby grown in buffered yeast extract (BYE) broth were
459 washed once with warm BYE broth to remove secreted proteins, adjusted to OD_{600} = 0.3 in 37 °C BYE
460 broth and incubated for 8 h at 37 °C and 250 rpm. OD_{600} was measured hourly, aliquots of the cultures
461 were adjusted to OD_{600} = 0.1 and supernatants were concentrated 100-fold by TCA precipitation. These
462 samples were analyzed in Western blots with antibodies directed against PlaA and ProA (27).
463

464 **Figure preparation**

465 Figures were prepared with Microsoft Power Point 2010 and Inkscape 0.92. All images, symbols and
466 fonts within the figures are acquired from Microsoft Power Point 2010. Images of crystal structures were
467 generated with PyMOL (70). Western Blots were labelled and processed with Adobe Photoshop CS6.
468 Graphs included in the Figures are visualized by Microsoft Excel 2010.

469

470 **Data availability statement**

471 All data generated or analyzed during this study are included in this published article or in the
472 supplementary information. Structures are available at PDBe with the accession codes 8A24 (PlaA iodide
473 SAD), 8A25 (PlaA complex with PEG fragment), and 8A26 (PlaA complex with palmitate). Note: The data
474 can be retrieved for review purposes from: https://nubes.helmholtz-berlin.de/s/rgfqBEiN3bHcxPe

475

476 **Supporting information**

477 This article contains supporting information.

478

479 **Acknowledgements**

480 We thank Susanne Karste, Ute Strutz, and Christian Galisch (Robert Koch-Institut) and Sabrina Groth
481 (Research Center Borstel) for excellent technical assistance. AF, TG, and WB, received funding from the
482 German Research Association (DFG) (FL359/6-1/2; priority program SPP2225 Exit Strategies of
483 Intracellular Pathogens FL359/10-1 and GU568/8-1; 281361126/GRK2223). We acknowledge the staff at
484 beamlines PXIII/X06DA at SLS (Paul Scherrer Institute, Villigen, Switzerland) and P11 (PETRAIII, DESY
485 Hamburg, Germany) for providing us access to their facilities.

486

487 **Authors contributions**

488 conceptualized the study: M.H., M.D., C.L., W.B., A.F.

489 supervised the study: W.B., A.F.

490 conceived and designed the experiments: M.H., M.D., S.W., C.L., W.B., A.F., T.G.

491 acquired data: M.H., M.D., S.W., C.L.

492 conducted the experiments: M.H., M.D., S.W., C.L.

493 analyzed the data: M.H., M.D., S.W., C.L., W.B., A.F., T.G.

494 interpreted the results: M.H., M.D., S.W., C.L., W.B., A.F., T.G.

495 drafted the manuscript: M.H., M.D., W.B., A.F.

496 revised the manuscript: M.H., M.D., S.W., C.L., W.B., A.F., T.G.

497 approved the final version: M.H., M.D., S.W., C.L., W.B., A.F., T.G.

498

499 **Data sharing**

500 All data generated or analyzed during this study are available in this article and the appendices.

501

502 **Declaration of Interests**

503 The authors declare that they have no conflicts of interest with the contents of this article.

504

505

506

507

508

509

510 **References**

511 1. Fields, B. S. (1996) The molecular ecology of legionellae. *Trends Microbiol.* **4**, 286-290
512 2. Mondino, S., Schmidt, S., Rolando, M., Escoll, P., Gomez-Valero, L., and Buchrieser, C. (2020)
513 Legionnaires' Disease: State of the Art Knowledge of Pathogenesis Mechanisms of Legionella.
514 3. Horwitz, M. A. (1983) The Legionnaires' disease bacterium (Legionella pneumophila) inhibits
515 phagosome-lysosome fusion in human monocytes. *The Journal of Experimental Medicine* **158**,
516 2108-2126
517 4. Finsel, I., and Hilbi, H. (2015) Formation of a pathogen vacuole according to Legionella
518 pneumophila: how to kill one bird with many stones. *Cell. Microbiol.* **17**, 935-950
519 5. Isberg, R. R., O'connor, T. J., and Heidtman, M. (2009) The Legionella pneumophila replication
520 vacuole: making a cosy niche inside host cells. *Nature Reviews Microbiology* **7**, 13-24
521 6. Segal, G., Purcell, M., and Shuman, H. A. (1998) Host cell killing and bacterial conjugation require
522 overlapping sets of genes within a 22-kb region of the Legionella pneumophila genome. *Proc.*
523 *Natl. Acad. Sci. U. S. A.* **95**, 1669-1674
524 7. Cianciotto, N. P. (2009) Many substrates and functions of type II secretion: lessons learned from
525 Legionella pneumophila. *Future Microbiol.* **4**, 797-805
526 8. White, R. C., and Cianciotto, N. P. (2019) Assessing the impact, genomics and evolution of type II
527 secretion across a large, medically important genus: the Legionella type II secretion paradigm.
528 *Microbial genomics* **5**
529 9. Burstein, D., Amaro, F., Zusman, T., Lifshitz, Z., Cohen, O., Gilbert, J. A., Pupko, T., Shuman, H. A.,
530 and Segal, G. (2016) Genomic analysis of 38 Legionella species identifies large and diverse
531 effector repertoires. *Nat. Genet.* **48**, 167
532 10. Gomez-Valero, L., Rusniok, C., Carson, D., Mondino, S., Pérez-Cobas, A. E., Rolando, M., Pasricha,
533 S., Reuter, S., Demirtas, J., and Crumbach, J. (2019) More than 18,000 effectors in the Legionella
534 genus genome provide multiple, independent combinations for replication in human cells.
535 *Proceedings of the National Academy of Sciences* **116**, 2265-2273
536 11. Gaspar, A. H., and Machner, M. P. (2014) VipD is a Rab5-activated phospholipase A1 that
537 protects Legionella pneumophila from endosomal fusion. *Proc. Natl. Acad. Sci. U. S. A.* **111**, 4560-
538 4565
539 12. VanRheenen, S. M., Luo, Z. Q., O'Connor, T., and Isberg, R. R. (2006) Members of a Legionella
540 pneumophila family of proteins with ExoU (phospholipase A) active sites are translocated to
541 target cells. *Infect. Immun.* **74**, 3597-3606
542 13. Shohdy, N., Efe, J. A., Emr, S. D., and Shuman, H. A. (2005) Pathogen effector protein screening in
543 yeast identifies Legionella factors that interfere with membrane trafficking. *Proc. Natl. Acad. Sci.*
544 *U. S. A.* **102**, 4866-4871
545 14. Li, X., Anderson, D. E., Chang, Y. Y., Jarnik, M., and Machner, M. P. (2022) VpdC is a ubiquitin-
546 activated phospholipase effector that regulates Legionella vacuole expansion during infection.
547 *Proc. Natl. Acad. Sci. U. S. A.* **119**, e2209149119
548 15. Creasey, E. A., and Isberg, R. R. (2012) The protein SdhA maintains the integrity of the Legionella-
549 containing vacuole. *Proc. Natl. Acad. Sci. U. S. A.* **109**, 3481-3486
550 16. Flieger, A., Frischknecht, F., Hacker, G., Hornef, M. W., and Pradel, G. (2018) Pathways of host
551 cell exit by intracellular pathogens. *Microb Cell* **5**, 525-544
552 17. Striednig, B., Lanner, U., Niggli, S., Katic, A., Vormittag, S., Brulisauer, S., Hochstrasser, R., Kaech,
553 A., Welin, A., Flieger, A., Ziegler, U., Schmidt, A., Hilbi, H., and Personnic, N. (2021) Quorum
554 sensing governs a transmissive Legionella subpopulation at the pathogen vacuole periphery.
555 *EMBO Rep* **22**, e52972

556 18. Flores-Diaz, M., Monturiol-Gross, L., Naylor, C., Alape-Giron, A., and Flieger, A. (2016) Bacterial
557 Sphingomyelinases and Phospholipases as Virulence Factors. *Microbiol. Mol. Biol. Rev.* **80**, 597-
558 628
559 19. Hiller, M., Lang, C., Michel, W., and Flieger, A. (2018) Secreted phospholipases of the lung
560 pathogen Legionella pneumophila. *Int. J. Med. Microbiol.* **308**, 168-175
561 20. Lang, C., and Flieger, A. (2011) Characterisation of Legionella pneumophila phospholipases and
562 their impact on host cells. *Eur. J. Cell Biol.* **90**, 903-912
563 21. Diwo, M., Michel, W., Aurass, P., Kuhle-Keindorf, K., Pippel, J., Krausze, J., Wamp, S., Lang, C.,
564 Blankenfeldt, W., and Flieger, A. (2021) NAD(H)-mediated tetramerization controls the activity of
565 Legionella pneumophila phospholipase PlaB. *Proc. Natl. Acad. Sci. U. S. A.* **118**
566 22. Akoh, C. C., Lee, G.-C., Liaw, Y.-C., Huang, T.-H., and Shaw, J.-F. (2004) GDSL family of serine
567 esterases/lipases. *Prog. Lipid Res.* **43**, 534-552
568 23. Upton, C., and Buckley, J. T. (1995) A new family of lipolytic enzymes? *Trends Biochem. Sci.* **20**,
569 178-179
570 24. Flieger, A., Gong, S., Faigle, M., Stevanovic, S., Cianciotto, N. P., and Neumeister, B. (2001) Novel
571 lysophospholipase A secreted by Legionella pneumophila. *J. Bacteriol.* **183**, 2121-2124
572 25. Flieger, A., Neumeister, B., and Cianciotto, N. P. (2002) Characterization of the gene encoding the
573 major secreted lysophospholipase A of Legionella pneumophila and its role in detoxification of
574 lysophosphatidylcholine. *Infect. Immun.* **70**, 6094-6106
575 26. Lang, C., Rastew, E., Hermes, B., Siegbrecht, E., Ahrends, R., Banerji, S., and Flieger, A. (2012) Zinc
576 metalloproteinase ProA directly activates Legionella pneumophila PlaC
577 glycerophospholipid:cholesterol acyltransferase. *J. Biol. Chem.* **287**, 23464-23478
578 27. Lang, C., Hiller, M., and Flieger, A. (2017) Disulfide loop cleavage of Legionella pneumophila PlaA
579 boosts lysophospholipase A activity. *Sci. Rep.* **7**, 16313
580 28. Choi, W. Y., Kim, S., Aurass, P., Huo, W., Creasey, E. A., Edwards, M., Lowe, M., and Isberg, R. R.
581 (2021) SdhA blocks disruption of the Legionella-containing vacuole by hijacking the OCRL
582 phosphatase. *Cell Rep* **37**, 109894
583 29. Flieger, A., Gong, S., Faigle, M., Northoff, H., and Neumeister, B. (2001) In vitro secretion kinetics
584 of proteins from Legionella pneumophila in comparison to proteins from non-pneumophila
585 species. *Microbiology* **147**, 3127-3134
586 30. Aurass, P., Gerlach, T., Becher, D., Voigt, B., Karste, S., Bernhardt, J., Riedel, K., Hecker, M., and
587 Flieger, A. (2016) Life Stage-specific Proteomes of Legionella pneumophila Reveal a Highly
588 Differential Abundance of Virulence-associated Dot/Icm effectors. *Mol. Cell. Proteomics* **15**, 177-
589 200
590 31. White, R. C., Gunderson, F. F., Tyson, J. Y., Richardson, K. H., Portlock, T. J., Garnett, J. A., and
591 Cianciotto, N. P. (2018) Type II Secretion-Dependent Aminopeptidase LapA and Acyltransferase
592 PlaC Are Redundant for Nutrient Acquisition during Legionella pneumophila Intracellular
593 Infection of Amoebas. *MBio* **9**
594 32. Dekker, N. (2000) Outer-membrane phospholipase A: known structure, unknown biological
595 function: MicroReview. *Mol. Microbiol.* **35**, 711-717
596 33. Kuhle, K., Krausze, J., Curth, U., Rossle, M., Heuner, K., Lang, C., and Flieger, A. (2014)
597 Oligomerization inhibits Legionella pneumophila PlaB phospholipase A activity. *J. Biol. Chem.*
598 **289**, 18657-18666
599 34. Bleffert, F., Granzin, J., Caliskan, M., Schott-Verdugo, S. N., Siebers, M., Thiele, B., Rahme, L.,
600 Felgner, S., Dormann, P., Gohlke, H., Batra-Safferling, R., Jaeger, K. E., and Kovacic, F. (2022)
601 Structural, mechanistic, and physiological insights into phospholipase A-mediated membrane
602 phospholipid degradation in Pseudomonas aeruginosa. *Elife* **11**
603 35. Aurass, P., Schlegel, M., Metwally, O., Harding, C. R., Schroeder, G. N., Frankel, G., and Flieger, A.
604 (2013) The Legionella pneumophila Dot/Icm-secreted effector PlcC/CegC1 together with PlcA

605 and PlcB promotes virulence and belongs to a novel zinc metallophospholipase C family present
606 in bacteria and fungi. *J. Biol. Chem.* **288**, 11080-11092
607 36. Banerji, S., Bewersdorff, M., Hermes, B., Cianciotto, N. P., and Flieger, A. (2005) Characterization
608 of the major secreted zinc metalloprotease- dependent glycerophospholipid:cholesterol
609 acyltransferase, PlaC, of Legionella pneumophila. *Infect. Immun.* **73**, 2899-2909
610 37. Qu, X., Song, X., Zhang, N., Ma, J., and Ge, H. (2020) The phospholipase A effector PlaA from
611 Legionella pneumophila: expression, purification and crystallization. *Acta Crystallogr F Struct Biol*
612 *Commun* **76**, 138-144
613 38. Vanaman, T. C., and Bradshaw, R. A. (1999) Proteases in cellular regulation minireview series. *J.*
614 *Biol. Chem.* **274**, 20047-20047
615 39. Holm, L. (2020) DALI and the persistence of protein shape. *Protein Sci.* **29**, 128-140
616 40. Pham, V. D., To, T. A., Gagne-Thivierge, C., Couture, M., Lague, P., Yao, D., Picard, M. E., Lortie, L.
617 A., Attere, S. A., Zhu, X., Levesque, R. C., Charette, S. J., and Shi, R. (2020) Structural insights into
618 the putative bacterial acetylcholinesterase ChoE and its substrate inhibition mechanism. *J. Biol.*
619 *Chem.* **295**, 8708-8724
620 41. Wan, Y., Liu, C., and Ma, Q. (2019) Structural analysis of a Vibrio phospholipase reveals an
621 unusual Ser-His-chloride catalytic triad. *J. Biol. Chem.* **294**, 11391-11401
622 42. van den Berg, B. (2010) Crystal Structure of a Full-Length Autotransporter. *J. Mol. Biol.* **396**, 627-
623 633
624 43. Anso, I., Basso, L. G. M., Wang, L., Marina, A., Paez-Perez, E. D., Jager, C., Gavotto, F., Tersa, M.,
625 Perrone, S., Contreras, F. X., Prandi, J., Gilleron, M., Linster, C. L., Corzana, F., Lowary, T. L.,
626 Trastoy, B., and Guerin, M. E. (2021) Molecular ruler mechanism and interfacial catalysis of the
627 integral membrane acyltransferase PatA. *Sci Adv* **7**, eabj4565
628 44. Scheithauer, L., Thiem, S., Schmelz, S., Dellmann, A., Bussow, K., Brouwer, R., Unal, C. M.,
629 Blankenfeldt, W., and Steinert, M. (2021) Zinc metalloprotease ProA of Legionella pneumophila
630 increases alveolar septal thickness in human lung tissue explants by collagen IV degradation. *Cell.*
631 *Microbiol.* **23**, e13313
632 45. Jumper, J., Evans, R., Pritzel, A., Green, T., Figurnov, M., Ronneberger, O., Tunyasuvunakool, K.,
633 Bates, R., Žídek, A., Potapenko, A., Bridgland, A., Meyer, C., Kohl, S. A. A., Ballard, A. J., Cowie, A.,
634 Romera-Paredes, B., Nikolov, S., Jain, R., Adler, J., Back, T., Petersen, S., Reiman, D., Clancy, E.,
635 Zielinski, M., Steinegger, M., Pacholska, M., Berghammer, T., Bodenstein, S., Silver, D., Vinyals,
636 O., Senior, A. W., Kavukcuoglu, K., Kohli, P., and Hassabis, D. (2021) Highly accurate protein
637 structure prediction with AlphaFold. *Nature* **596**, 583-589
638 46. Khan, F. I., Lan, D., Durrani, R., Huan, W., Zhao, Z., and Wang, Y. (2017) The Lid Domain in
639 Lipases: Structural and Functional Determinant of Enzymatic Properties. *Frontiers in*
640 *bioengineering and biotechnology* **5**, 16-16
641 47. Gordon, V. M., and Leppla, S. H. (1994) Proteolytic activation of bacterial toxins: role of bacterial
642 and host cell proteases. *Infect. Immun.* **62**, 333-340
643 48. Kurmanova, A., Llorente, A., Polesskaya, A., Garred, Ø., Olsnes, S., Kozlov, J., and Sandvig, K.
644 (2007) Structural requirements for furin-induced cleavage and activation of Shiga toxin. *Biochem.*
645 *Biophys. Res. Commun.* **357**, 144-149
646 49. Ogata, M., Fryling, C., Pastan, I., and FitzGerald, D. (1992) Cell-mediated cleavage of
647 Pseudomonas exotoxin between Arg279 and Gly280 generates the enzymatically active fragment
648 which translocates to the cytosol. *J. Biol. Chem.* **267**, 25396-25401
649 50. van Deurs, B., and Sandvig, K. (1995) Furin-induced cleavage and activation of Shiga toxin. *J. Biol.*
650 *Chem.* **270**, 10817-10821
651 51. Veldhuizen, R., Nag, K., Orgeig, S., and Possmayer, F. (1998) The role of lipids in pulmonary
652 surfactant. *Biochim. Biophys. Acta* **1408**, 90-108

653 52. Laguna, R. K., Creasey, E. A., Li, Z., Valtz, N., and Isberg, R. R. (2006) A Legionella pneumophila-
654 translocated substrate that is required for growth within macrophages and protection from host
655 cell death. *Proceedings of the National Academy of Sciences* **103**, 18745-18750
656 53. Ruiz-Albert, J., Yu, X. J., Beuzón, C. R., Blakey, A. N., Galyov, E. E., and Holden, D. W. (2002)
657 Complementary activities of SseJ and SifA regulate dynamics of the Salmonella typhimurium
658 vacuolar membrane. *Mol. Microbiol.* **44**, 645-661
659 54. Roy, C. R. (2012) Vacuolar pathogens value membrane integrity. *Proc. Natl. Acad. Sci. U. S. A.*
660 **109**, 3197-3198
661 55. Miller, M. B., and Bassler, B. L. (2001) Quorum sensing in bacteria. *Annu. Rev. Microbiol.* **55**, 165-
662 199
663 56. Edelstein, P. H. (1981) Improved semiselective medium for isolation of Legionella pneumophila
664 from contaminated clinical and environmental specimens. *J. Clin. Microbiol.* **14**, 298-303
665 57. Bertani, G. (1951) Studies on lysogenesis. I. The mode of phage liberation by lysogenic
666 Escherichia coli. *J. Bacteriol.* **62**, 293-300
667 58. Bingel-Erlenmeyer, R., Olieric, V., Grimshaw, J. P. A., Gabadinho, J., Wang, X., Ebner, S. G.,
668 Isenegger, A., Schneider, R., Schneider, J., Glettig, W., Pradervand, C., Panepucci, E. H., Tomizaki,
669 T., Wang, M., and Schulze-Briese, C. (2011) SLS Crystallization Platform at Beamline X06DA—A
670 Fully Automated Pipeline Enabling in Situ X-ray Diffraction Screening. *Crystal Growth & Design*
671 **11**, 916-923
672 59. Vonrhein, C., Flensburg, C., Keller, P., Sharff, A., Smart, O., Paciorek, W., Womack, T., and
673 Bricogne, G. (2011) Data processing and analysis with the autoPROC toolbox. *Acta Crystallogr. D*
674 *Biol. Crystallogr.* **67**, 293-302
675 60. Pape, T., and Schneider, T. R. (2004) HKL2MAP: a graphical user interface for macromolecular
676 phasing with SHELX programs. *Journal of Applied Crystallography* **37**, 843-844
677 61. Terwilliger, T. C., Grosse-Kunstleve, R. W., Afonine, P. V., Moriarty, N. W., Zwart, P. H., Hung, L.-
678 W., Read, R. J., and Adams, P. D. (2008) Iterative model building, structure refinement and
679 density modification with the PHENIX AutoBuild wizard. *Acta Crystallographica Section D* **64**, 61-
680 69
681 62. Emsley, P., Lohkamp, B., Scott, W. G., and Cowtan, K. (2010) Features and development of Coot.
682 *Acta Crystallogr. D Biol. Crystallogr.* **66**, 486-501
683 63. Winn, M. D., Ballard, C. C., Cowtan, K. D., Dodson, E. J., Emsley, P., Evans, P. R., Keegan, R. M.,
684 Krissinel, E. B., Leslie, A. G., McCoy, A., McNicholas, S. J., Murshudov, G. N., Pannu, N. S.,
685 Potterton, E. A., Powell, H. R., Read, R. J., Vagin, A., and Wilson, K. S. (2011) Overview of the
686 CCP4 suite and current developments. *Acta Crystallogr. D Biol. Crystallogr.* **67**, 235-242
687 64. Joosten, R. P., Long, F., Murshudov, G. N., and Perrakis, A. (2014) The PDB_REDO server for
688 macromolecular structure model optimization. *IUCrJ* **1**, 213-220
689 65. Afonine, P. V., Grosse-Kunstleve, R. W., Echols, N., Headd, J. J., Moriarty, N. W., Mustyakimov,
690 M., Terwilliger, T. C., Urzhumtsev, A., Zwart, P. H., and Adams, P. D. (2012) Towards automated
691 crystallographic structure refinement with phenix.refine. *Acta Crystallogr. D Biol. Crystallogr.* **68**,
692 352-367
693 66. Burkhardt, A. (2016) Status of the crystallography beamlines at PETRA III. *Eur. Phys. J. Plus* **131**
694 67. Mirdita, M., Schutze, K., Moriwaki, Y., Heo, L., Ovchinnikov, S., and Steinegger, M. (2022)
695 ColabFold: making protein folding accessible to all. *Nat Methods* **19**, 679-682
696 68. Flieger, A., Gongab, S., Faigle, M., Mayer, H. A., Kehrer, U., Mussotter, J., Bartmann, P., and
697 Neumeister, B. (2000) Phospholipase A secreted by Legionella pneumophila destroys alveolar
698 surfactant phospholipids. *FEMS Microbiol. Lett.* **188**, 129-133
699 69. Schromm, A. B., Brandenburg, K., Rietschel, E. T., Flad, H. D., Carroll, S. F., and Seydel, U. (1996)
700 Lipopolysaccharide-binding protein mediates CD14-independent intercalation of
701 lipopolysaccharide into phospholipid membranes. *FEBS Lett.* **399**, 267-271

702 70. Schrödinger, LLC. (2020) The PyMOL Molecular Graphics System, Version 2.4.
703 71. Jepras, R., Fitzgeorge, R., and Baskerville, A. (1985) A comparison of virulence of two strains of
704 Legionella pneumophila based on experimental aerosol infection of guinea-pigs. *Epidemiol.*
705 *Infect.* **95**, 29-38
706

707 **Abbreviations:**

708 CTD	C-terminal domain
709 ePC	L-α-phosphatidylcholine (chicken egg)
710 ecPE	L-α-phosphatidylethanolamine (*E. coli*)
711 FFA	free fatty acids
712 FRET	Förster-Resonance-Energy-Transfer
713 GCAT	glycerophospholipid:cholesterol acyltransferase
714 LCV	*Legionella*-containing vacuole
715 LPC or 16:0 LPC	1-monopalmitoyllysophosphatidylcholine
716 LPG	1-mono-palmitoyllysophosphatidylglycerol
717 LPLA	lysophospholipase A
718 NBD-PE	*N*-(7-nitrobenz-2-oxa-1,3-diazol-4-yl)-1,2-dihexadecanoyl-*sn*-
719	glycero-3-phosphoethanolamine
720 MW	molecular weight
721 PC	1,2-dipalmitoylphosphatidylcholine
722 PEG	polyethylene glycol
723 PG	1,2-dipalmitoylphosphatidyl-glycerol
724 PLA/PLB/PLC/PLD	phospholipase A/B/C/D
725 Rho-DHPE	Lissamine™ Rhodamine B 1,2-dihexadecanoyl-*sn*-
726	glycero-3-phosphoethanolamine
727 SAD	single anomalous dispersion
728 SEC	size exclusion chromatography
729 SP	signal peptide
730 T2SS/T4SS	type II/IV secretion system
731 8:0 LPC	1-monooctanoyllysophosphatidylcholine
732 12:0 LPC	1-monolauroyllysophosphatidylcholine
733 18:0 LPC	1-monostearoyllysophosphatidylcholine
734 20:0 LPC	1-monoarachidoyllysophosphatidylcholine

22:0 LPC	1-monobehenoyllysophosphatidylcholine	

Tables

Table 1: Comparison of protein properties of *L. pneumophila* GDSL enzymes PlaA, PlaC, and PlaD; CTD – presence of additional C-terminal domain

Protein property	PlaA (lpc1811)	PlaC (lpc3121)	PlaD (lpc0558)
Size / SP [AA]	18 / 309	24 / 433	519
MW [kDa]	34.4	49.7	59.6
MW w/o SP [kDa]	32.8	46.9	no signal peptide
MW w/o SP [kDa], processed	25.3	36.1	no processing
Catalytic triad	S30, D279, H282	S37, D398, H401	S17, D341, H344
Central β-sheet	5 parallel	5 parallel	5 parallel + 1 antiparallel
additional helices in α/β-hydrolase fold	No	yes (P57-G120 and D166-P193)	no
Lid	yes (C243-C272)	yes (C343-C388)	no lid and no disulfide loop
CTD	No	no	yes (K400-T516)

Table 2: Overview of strains used in this study.

* -(SP): constructs cloned without sequence coding for the putative signal peptide (aa 1-18), strain was used for PlaA expression and purification for crystallization, X-ray diffraction, and structure determination.

Organism	**Mutation/Plasmid**	**Tag**	**Selection marker**	**Reference**
L. pn. Corby	Wild type	-	-	(71)
E. coli BL21 (pCL119)	pGP172 $plaA_{Corby}$ (-SP)*	N-term. Strep-tag	Amp^R	(27)
E. coli BL21 (pCL121)	pGP172 $plaA_{Corby}$ S30N (-SP)	N-term. Strep-tag	Amp^R	(27)
E. coli BL21 (pCL126)	pGP172 $plaA_{Corby}$ ΔAA248-67(-SP)	N-term. Strep-tag	Amp^R	(27)
E. coli BL21 (pCL127)	pGP172 $plaA_{Corby}$ S30N ΔAA248-67 (-SP)	N-term. Strep-tag	Amp^R	(27)
E. coli BL21 (pMH41)	pGP172 $plaA_{Corby}$ E266N L267N (-SP)	N-term. Strep-tag	Amp^R	(27)
E. coli BL21 (pMH42)	pGP172 $plaA_{Corby}$ S30N E266N L267N (-SP)	N-term. Strep-tag	Amp^R	This study
E. coli BL21 (pCL15)	pet28a(+) $proA_{Corby}$	N-term. Strep-tag	Km^R	(26)

751

752 **Table 3:** X-ray data collection and refinement statistics.

Structure	PlaA iodide SAD	PlaA PEG complex	PlaA palmitate complex
PDB-ID:	8A24	8A25	8A26
Data collection[a]			
Beamline	SLS X06DA (PXIII; 2018/02/22)	SLS X06DA (PXIII; 2018/02/22)	PetraIII P11 (2018/05/29)
Wavelength (Å)	1.7712	1.3778	1.00
Space group	$P3_121$	$P3_121$	$P3_121$
Cell dimensions			
a, *b*, *c* (Å)	81.85, 81.85, 68.21	82.24, 82.24, 68.45	82.92, 82.92, 68.64
α, β, γ (°)	90, 90, 120	90, 90, 120	90, 90, 120
Resolution (Å)[b]	70.89 – 2.36 (2.41 – 2.36)	49.35 – 1.73 (1.76 – 1.73)	49.62 – 1.45 (1.48 – 1.45)
R_{merge} (%)[b]	18.9 (196.2)	6.4 (140.5)	6.3 (160.0)
R_{pim} (%)[b]	3.1 (32.1)	1.5 (32.3)	1.1 (29.6)
$I/\sigma(I)$[b]	21.4 (2.3)	28.5 (2.2)	33.6 (2.3)
Completeness (%)[b]	100.0 (100.0)	96.0 (100)	100.0 (100.0)
Redundancy[b]	38.4 (37.5) anomalous: 20.4 (19.5)	19.2 (19.8)	32.8 (29.8)
$CC_{1/2}$ (%)[b]	99.9 (83.9)	100 (74.4)	100 (82.3)
Refinement			
Resolution (Å)[b]	70.89 - 2.36 (2.45 - 2.36)	49.35 – 1.73 (1.79 – 1.73)	49.62 – 1.45 (1.50 – 1.45)
No. reflections[b]	11124 (1079)	27072 (2801)	48590 (4808)
R_{work} (%)[b]	22.81 (27.67)	15.96 (23.84)	15.55 (25.83)
R_{free} (%)[b]	27.91 (28.90)	18.54 (28.75)	17.74 (26.92)
No. atoms			
Protein	2206	2297	2319
Ligand/ion	13	59	115
Water	62	168	225
B-factors (Å^2)			
Protein	54	35	25
Ligand/ion	90	51	46
Water	53	39	37
R.m.s deviations			
Bond lengths (Å)	0.002	0.005	0.006
Bond angles (º)	0.44	0.800	0.930
Ramachandran			
Favored	94.6	97.21	97.19
Allowed	5.04	2.79	2.81
Outliers	0.36	0.00	0.00

753 [a]Values for the highest resolution shell are shown in parentheses.
754 [a]Data were indexed, integrated, scaled and merged with autoproc. The statistics reported here result from isotropic treatment,
755 using I/σ(I) > 2.0 as a high resolution cut-off.
756
757
758
759

760 **Figure Legends**

761

762 **Figure 1: Crystal structure of *Legionella pneumophila* PlaA in complex with palmitic acid shows that**
763 **the disulfide loop covers the catalytic triade.** (*A*) cartoon representation of PlaA, colored from blue at
764 the N-terminus to red at the C-terminus. Important residues of the active site (catalytic triad: S30, D279,
765 H282) and the limiting residues (C243, C272) of the disulfide loop (orange) are shown as sticks (carbon:
766 yellow, oxygen: red, nitrogen: blue, sulfur: gold), together with the product palmitic acid (carbon: black).
767 The ProA cleavage site resides within the disulfide loop. (*B*) cross-eyed stereoplot of the substrate
768 binding site. Palmitic acid is shown in black, the ligand binding cavity is shown in grey. Residues that
769 contribute to the binding site are shown as sticks (carbon: green). (*C*) surface representation of PlaA. The
770 protein is in the same orientation as in *A*. Note that the disulfide loop shown in yellow shields the active
771 site fully.

772

773 **Figure 2: Crystal structures of selected proteins related to *L. pneumophila* PlaA according to analysis**
774 **with DALI** (39)**.** Ribbon representations with residues of the catalytic triad in the active site are shown as
775 sticks on the left; top views of the molecular surface are shown on the right. Residues of the disulfide
776 loops are plotted in yellow. Oxygen and nitrogen atoms of the catalytic triad are shown in red and blue,
777 respectively. (*A*) Crystal structure of *L. pneumophila* in complex with palmitic acid. (*B*) *P. aeruginosa* ChoE
778 is an acetylcholinesterase (PDB entry 1uqv) (40). (*C*) *V. vulnificus* PlpA is a type II-secreted phospholipase
779 A2 that utilizes a chloride ion (green sphere) instead of aspartate in its catalytic triad (PDB entry 6jkz)
780 (41). (*D*) EstA is an autotransported esterase displayed on the outer membrane of *P. aeruginosa*. The
781 autotransporter domain is shown in darker colors (PDB entry 3kvn) (42). Note that ChoE, PlpA and EstA
782 have significantly shorter disulfide loops than PlaA, which makes their active sites solvent-accessible.

783

784 **Figure 3: Deletion of the disulfide loop in PlaA increases membrane interaction.** Protein-membrane
785 insertion of PlaA S30N and disulfide loop deletion mutant PlaA S30N Δaa247-268 was monitored by FRET
786 spectroscopy. An increase of the intensity ratio $I_{donor}/I_{acceptor}$ corresponds to a reduced FRET efficiency and
787 indicates insertion of proteins into the ePC:ecPE (1:1) liposomes. Experiments were performed in 40 mM
788 Tris, 150 mM NaCl, pH 7.5, at 37 °C. Values were determined 60 min after addition of 100 µg/ml protein.
789 Two of three representative experiments are shown. Open and closed circles refer to data points of
790 different experiments.

791

792 **Figure 4: PlaA prefers lysophospholipids with 16:0 fatty acid chains for hydrolysis, processing of PlaA in**
793 **liquid culture occurs from mid-logarithmic growth, and ProA processing site E266/L267 in PlaA is not**
794 **essential for enzyme activation.** (*A, E*) PLA and LPLA activities of PlaA and PlaA variants were determined
795 via quantification of free fatty acids (FFA) after incubation for 3 h with the indicated lipids at 37 °C *(B)*
796 The growth of *L. pneumophila* wild type in broth was monitored over a period of 7 h and samples of
797 culture supernatants were analyzed for the presence and *(C)* processing status of PlaA and *(D)* presence
798 of ProA by Western blotting with PlaA- and ProA-directed antibodies, respectively. Molecular weight
799 standards are shown on the left of the Western blots. The data are representative for one additional
800 experiment. In (*E*) 16:0 phospholipids were used for all lipid species and reactions were performed
801 without or with addition of 3.5 mU ProA as indicated. (*A, E*) Data are shown as mean and standard
802 deviation (n=2) and are representative for three additional experiments.
803
804 **Figure 5: AlphaFold** (45) **predicted structures of the three *L. pneumophila* GDSL phospholipases PlaA,**
805 **PlaC, and PlaD.** Representations, orientations and color schemes are similar to Fig. 2. (*A*) AlphaFold
806 model of PlaA. Note the correct prediction of the position of the disulfide loop with respect to the
807 experimental structure (compare to Fig. 2A and Fig. S2A-C), leading to a shielded active site. (*B*)
808 AlphaFold model of PlaC. The predicted position of the disulfide loop leads to a similar shielding as in
809 PlaA. (*C*) AlphaFold model of PlaD. PlaD does not contain a disulfide loop; residues structurally
810 corresponding to the disulfide loop of PlaA are shown in light blue. The predicted additional C-terminal
811 domain of unknown function of PlaD is shown in light green. Note that the active site of PlaD is predicted
812 to be solvent-exposed, however, the C-terminal domain may position itself to block access to the active
813 center.
814
815
816

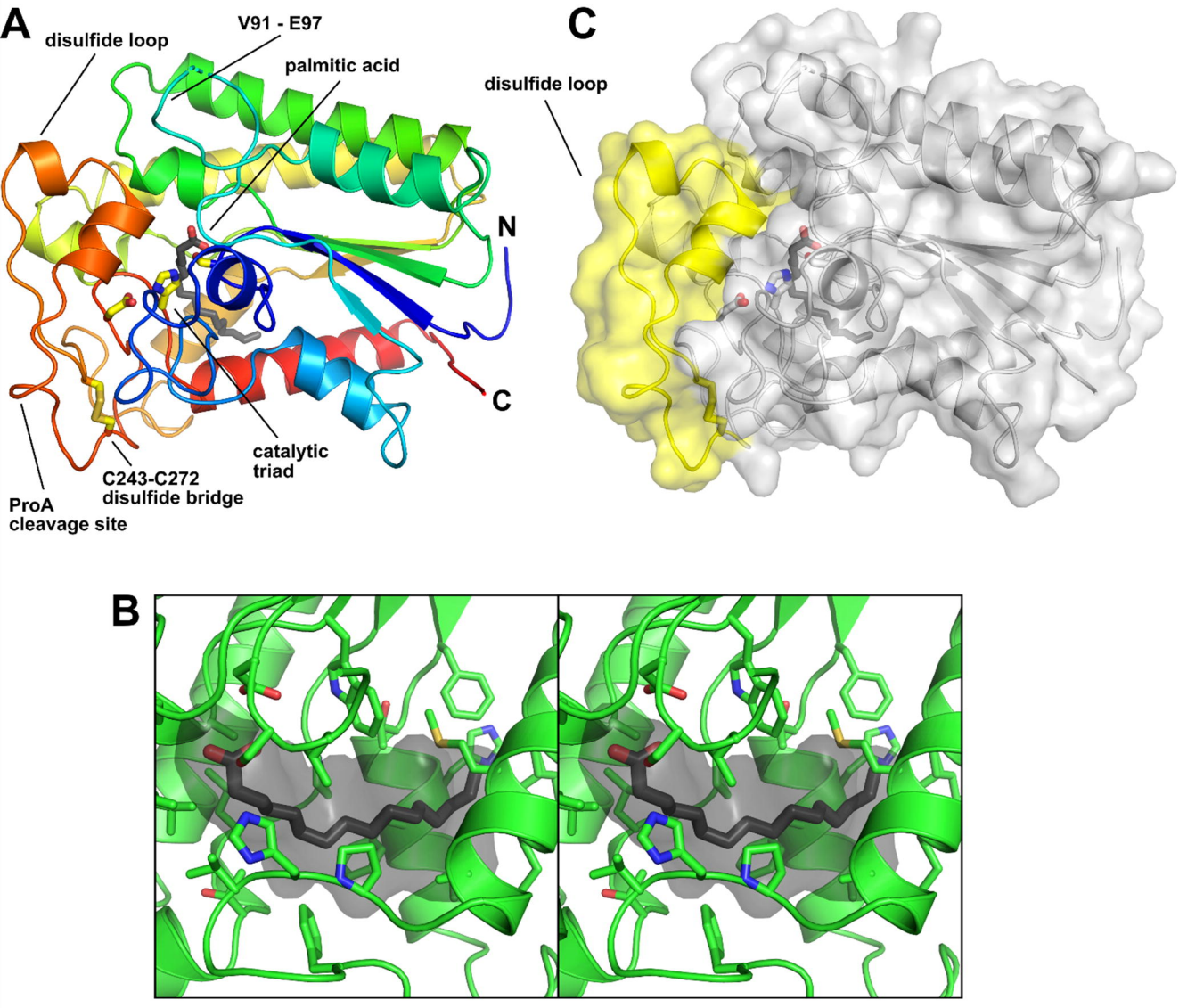
A
disulfide loop
V91 - E97
palmitic acid
N
C
catalytic
triad
C243-C272
disulfide bridge
ProA
cleavage site
C
disulfide loop
B

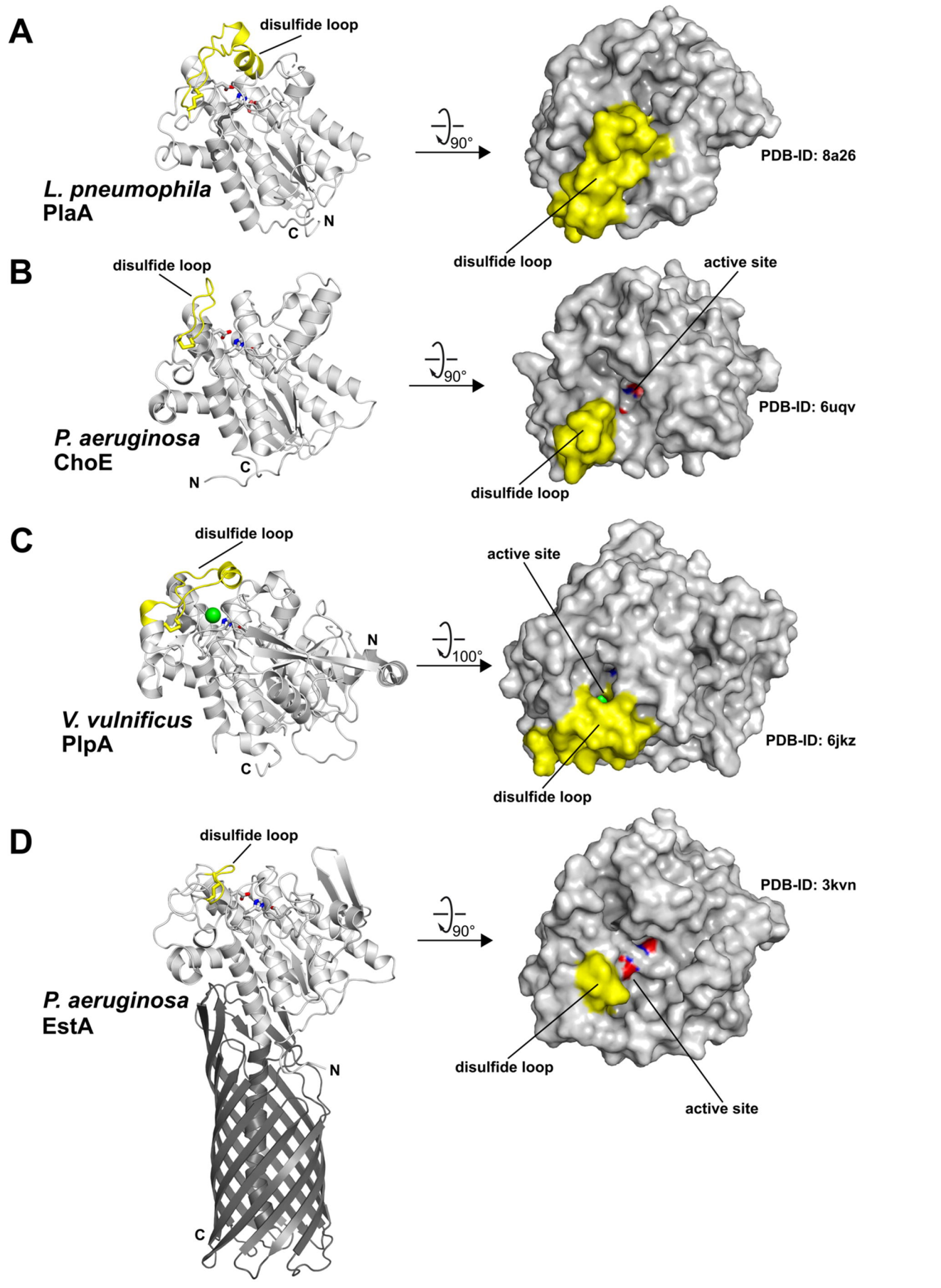
A
disulfide loop
L. pneumophila
PlaA
C
N
90°
PDB-ID: 8a26
disulfide loop
B
disulfide loop
P. aeruginosa
ChoE
C
N
90°
active site
PDB-ID: 6uqv
disulfide loop
C
disulfide loop
N
V. vulnificus
PlpA
C
100°
active site
PDB-ID: 6jkz
disulfide loop
D
disulfide loop
P. aeruginosa
EstA
N
C
90°
PDB-ID: 3kvn
disulfide loop
active site

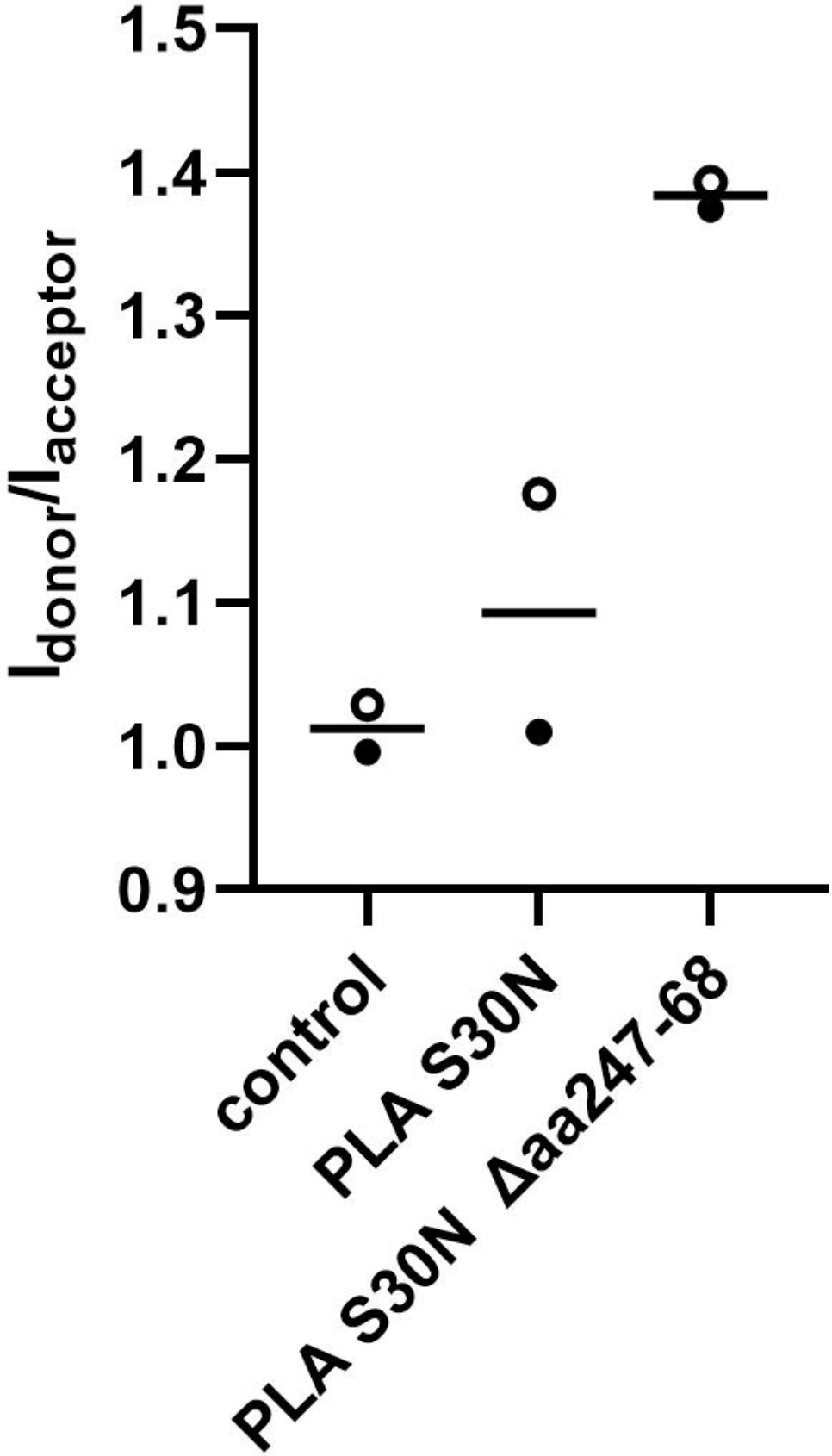
1.5
1.4
1.3
1.2
1.1
1.0
0.9
$I_{donor}/I_{acceptor}$
control
PLA S30N
PLA S30N Δaa247-68

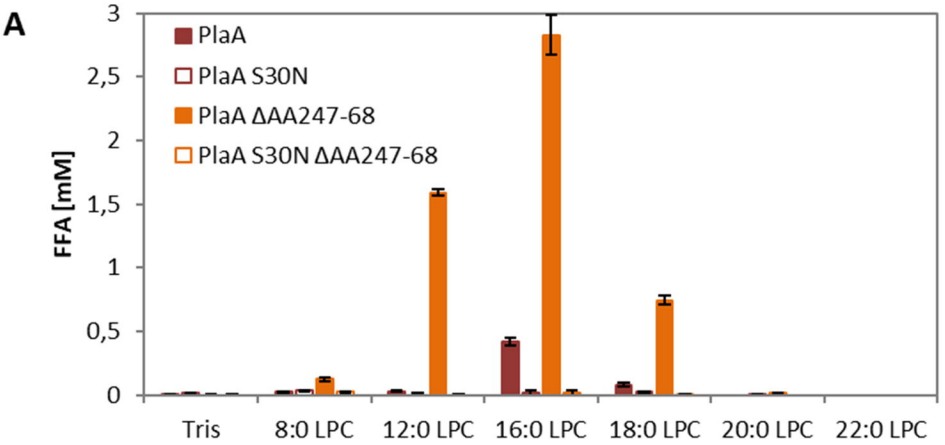
A
PlaA
PlaA S30N
PlaA ΔAA247-68
PlaA S30N ΔAA247-68
FFA [mM]
3
2,5
2
1,5
1
0,5
0
Tris
8:0 LPC
12:0 LPC
16:0 LPC
18:0 LPC
20:0 LPC
22:0 LPC

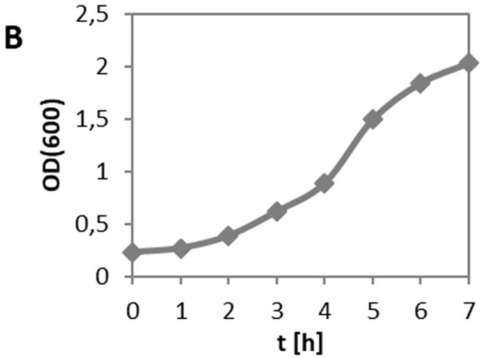
B
OD(600)
2,5
2
1,5
1
0,5
0
0
1
2
3
4
5
6
7
t [h]

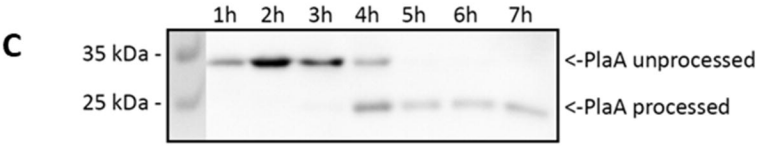
C
1h
2h
3h
4h
5h
6h
7h
35 kDa -
25 kDa -
<-PlaA unprocessed
<-PlaA processed

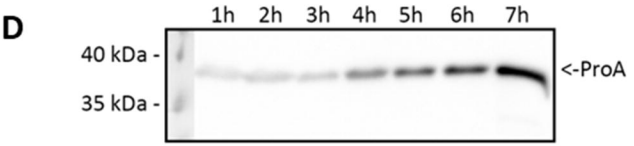
D
1h
2h
3h
4h
5h
6h
7h
40 kDa -
35 kDa -
<-ProA

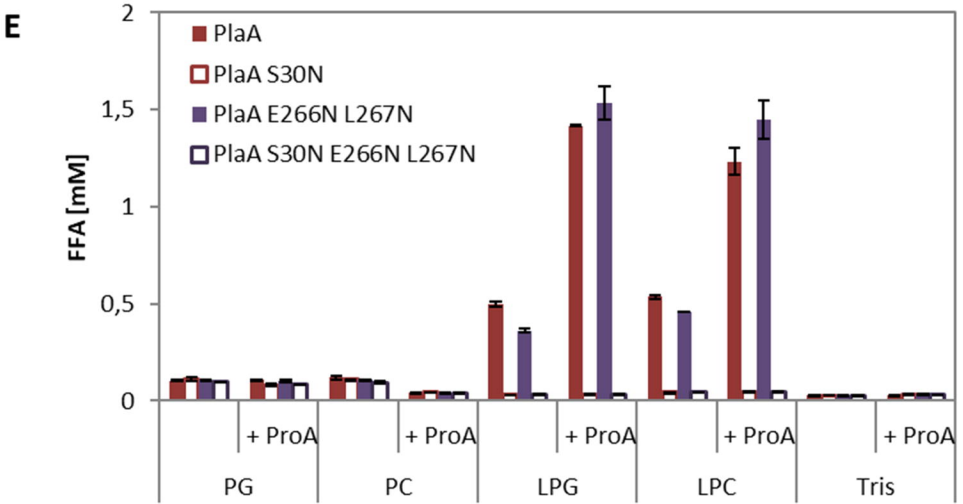
E
PlaA
PlaA S30N
PlaA E266N L267N
PlaA S30N E266N L267N
FFA [mM]
2
1,5
1
0,5
0
+ ProA
+ ProA
+ ProA
+ ProA
+ ProA
PG
PC
LPG
LPC
Tris